EVTeC 2023
6th International Electric Vehicle Technology Conference 2023

20231081

Effective Modeling and Controller Design for Two-Input-Two-Output Torque Difference Amplification Motor Drive System

Hiroyuki Fuse[1)] **Guangzhi Yu**[1)] **Hiroshi Fujimoto**[1)] **Kaoru Sawase**[2)]
Naoki Takahashi[2)] **Ryota Takahashi**[2)] **Yutaro Okamura**[2)] **Ryosuke Koga**[2)]

1) The University of Tokyo, 5-1-5 Kashiwanoha, Kashiwa, Chiba, 277-8561 Japan
2) MITSUBISHI MOTORS CORPORATION, 1, Nakashinkiri, Hashimecho, Okazaki, Aichi, 444–8501, Japan
E-mail: fuse@edu.k.u-tokyo.ac.jp

ABSTRACT: For electrified vehicles, a torque vectoring differential (TVD) with a two-motor-torque difference amplification mechanism (TDA-TVD) has been proposed and it generates a greater torque difference. However, due to the complex driving force transmission system including planetary gears and driveshafts, TDA-TVD has problems with the vibration of both the driveshaft torque and the yaw rate while differential torque is generated. To deal with this issue, this study analyzes TDA-TVD in frequency domain and also propose a novel modeling method to construct vibration suppression controllers that deal with both longitudinal motion and yaw motion simultaneously. First, this paper shows a theoretical frequency domain analysis using matrices and obtain resonance frequencies of TDA-TVD. Second, TDA-TVD is modeled based on a summation-differential mode transformation. Third, simulations and experimental evaluations of vibration suppression using a real vehicle with the TDA-TVD are demonstrated.

KEY WORDS: Electric Vehicle, Motor Drive System, Two-Input-Two-Output System, Vibration Suppression, Decoupling Compensation, Torque Vectoring Differential

Nomenclature

M	Vehicle mass
r	Effective wheel radius
J_ω, J_M, J_L	Wheel, Motor, and Nominal load inertia
G	Primary reduction gear ratio
b_1, b_2	Equivalent secondary reduction gear ratio
K_s	Stiffness of driveshaft
D_s, D_M, D_L	Damping factor of driveshaft, motor, and wheel
$T_{R(L)M}$	Input motor torque (R: right side, L: left side)
$T_{R(L)Dm}$	Input motor torque after primary gear reduction
$T_{R(L)m}$	Transmitted motor torque to planetary gears
$T_{R(L)in}$	Input motor torque converted to driveshaft side
$T_{R(L)ds}$	Driveshaft torque after secondary gear reduction
$T_{R(L)L}$	Load torque
$\omega_{R(L)M}$	Motor side angular speed before gear reduction
$\omega_{R(L)m}$	Motor side angular speed after gear reduction
$\omega_{R(L)ds}$	Driveshaft side angular speed
$\omega_{R(L)L}$	Wheel angular speed
λ	slip ratio

1. Introduction

Torque vectoring differential (TVD) is a device that controls direct yaw moment by generating a torque difference between the left and right wheels. TVD has the advantage to improve the cornering performance by actively controlling the yaw moment [(1) (2) (6)].

For that reason, some electric vehicles adopt individual-wheel-drive (IWD) systems (either with on-board or in wheel motor) and a lot of torque vectoring or distribution algorithms have been studied [(3) (7)]. However, available maximum torque difference and direct yaw moment decrease when the vehicle is at high speed, and the same problem occurs when the vehicle is cornering near the critical region, due to the decreased traction of the inner wheels caused by the load transfer.

A TVD with a two-motor-torque difference amplification mechanism (TDA-TVD) has been proposed in order to increase the available maximum torque difference [(4) (5)]. TDA-TVD drives two wheels with two motors, but unlike conventional IWD vehicles, there is a mechanical coupling between the left and right wheels as seen in Fig. 1. Therefore, TDA-TVD is categorized as the two-input-two-output drive system. Thanks to the mechanical coupling, TDA-TVD can generates greater torque differences between the left and right wheels compared to the conventional IWD system with the same electric traction motor. However, while TDA-TVD has the same advantages as the TVD, it has relatively complex mechanical components, including planetary gears, reduction gears, and driveshafts. This leads to undesirable vibrations of the driveshaft torque on the wheels and yaw rate vibration while cornering with its torque vectoring system in function. The previous study [(4) (5)] did not derive the dynamic model of TDA-TVD that describes its anticipated vibrations of the driveshaft torque and yaw motion. These problems limit the performance of TDA-TVD and must be solved.

To deal with this issue, a previous study derived a linearized model of TDA-TVD and designed a vibration suppression feedforward controller [(8)]. The derived linearized model assumed a constant load model (when vehicle is going on straight paths), which does not guarantee its performance for any situations (e.g., cornering). Furthermore, the parameter tuning of the vibration suppression controller was based on time-domain analysis (i.e., waveform of measured driveshaft torque).

On the other hand, this study first analyzes TDA-TVD in the frequency domain in detail, clarifying resonance frequencies and corresponding vibration modes. Second, this study proposes a novel linearized model of TDA-TVD that well describes the longitudinal motion and yaw motion using a coordinate transforma-

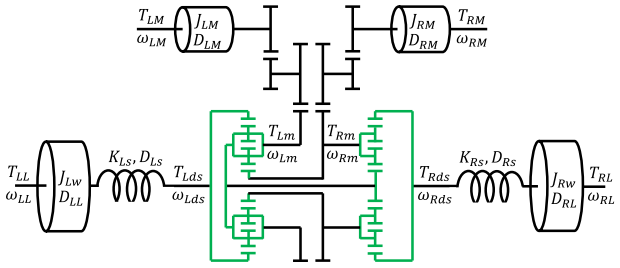

Fig. 1 Schematic diagram of TDA-TVD [5].

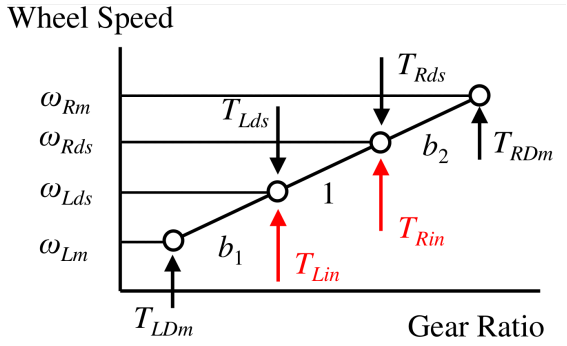

Fig. 2 Speed diagram of TDA-TVD.

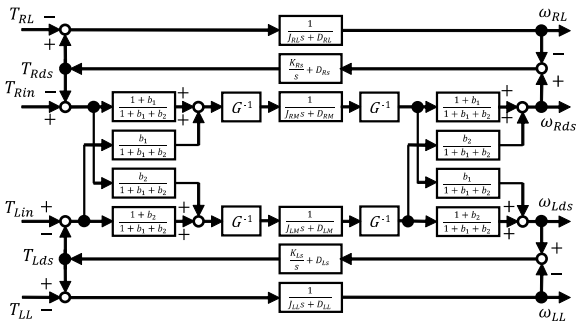

Fig. 3 Block diagrams of linearized normal model of TDA-TVD.

tion. By doing this, a frequency domain analysis of the real hardware of TDA-TVD will be much easier. Furthermore, the driveshaft torque vibration of the longitudinal and yaw modes could be effectively mitigated by designing controllers for the corresponding modes.

2. Dynamic model of TDA-TVD

Several types of TDA-TVD have been proposed by Sawase [4] [5]. As an example of those, a schematic diagram of TDA-TVD is shown in Fig. 1. Regardless of the difference of the types of TDA-TVD, the major function of differential torque amplification can be represented using b_1 and b_2 as shown in Fig. 2 [5]. In the figure, b_1 and b_2 are the equivalent secondary reduction gear ratios determined by each gear of the planetary gears. b_1 and b_2 are designed to be as equal as possible. From these two figures, the group of the authors derived a dynamic model of TDA-TVD as shown in Fig. 3 [8], which is called normal mode in this paper.

The previously proposed normal mode modeling requires relatively complex additional controller to suppress the vibration since there are two resonance modes.

2.1. Derivation of Dynamic Model of TDA-TVD on Normal Mode

In Fig. 3, motor torque and angular speeds are chosen as inputs and outputs, but converted to the driveshaft side (for example, the input motor torque $\boldsymbol{T_M}$ is converted to a driveshaft side torque input $\boldsymbol{T_{in}}$, which is shown in (5)). This is convenient to control the driveshaft side angular wheel speed $\omega_{R(L)ds}$ and driveshaft torque $T_{R(L)ds}$.

In the previous study, vectors and matrices are partly used to derive the dynamic model of TDA-TVD, but in this study, they are fully employed for simpler and more organized representation. The following three equations represent the dynamics of the left and right wheels, motors, and driveshafts as follows

$$\boldsymbol{\omega_L} = \boldsymbol{P_L}(\boldsymbol{T_{ds}} - \boldsymbol{T_L}) \tag{1}$$
$$\boldsymbol{\omega_{ds}} = \boldsymbol{B}^{-1}\boldsymbol{G}^{-1}\boldsymbol{P_M}\boldsymbol{G}^{-1}(\boldsymbol{B}^T)^{-1}(\boldsymbol{T_{in}} - \boldsymbol{T_{ds}}) \tag{2}$$
$$\boldsymbol{T_{ds}} = \boldsymbol{P_{ds}}(\boldsymbol{\omega_{ds}} - \boldsymbol{\omega_L}) \tag{3}$$

where

$$\begin{pmatrix}\boldsymbol{\omega_L} & \boldsymbol{\omega_{ds}} & \boldsymbol{T_L} & \boldsymbol{T_{ds}}\end{pmatrix} = \begin{pmatrix}\omega_{RL} & \omega_{Rds} & T_{LL} & T_{Lds} \\ \omega_{LL} & \omega_{Lds} & T_{RL} & T_{Rds}\end{pmatrix} \tag{4}$$

$$\boldsymbol{T_{in}} = \boldsymbol{B}\boldsymbol{G}\boldsymbol{T_M} \tag{5}$$
$$\begin{pmatrix}T_{Rin} \\ T_{Lin}\end{pmatrix} = \begin{pmatrix}b_2+1 & -b_2 \\ -b_1 & b_1+1\end{pmatrix}\begin{pmatrix}G_R & 0 \\ 0 & G_L\end{pmatrix}\begin{pmatrix}T_{RM} \\ T_{LM}\end{pmatrix}$$
$$\boldsymbol{\omega_{ds}} = \boldsymbol{B}^{-1}\boldsymbol{G}\boldsymbol{\omega_M} \tag{6}$$

$$\boldsymbol{P_L} = \begin{pmatrix}\frac{1}{J_{RL}s+D_{RL}} & 0 \\ 0 & \frac{1}{J_{LL}s+D_{LL}}\end{pmatrix} \tag{7}$$

$$\boldsymbol{P_M} = \begin{pmatrix}\frac{1}{J_{RM}s+D_{RM}} & 0 \\ 0 & \frac{1}{J_{LM}s+D_{LM}}\end{pmatrix} \tag{8}$$

$$\boldsymbol{P_{ds}} = \begin{pmatrix}D_{Rs}+\frac{K_{Rs}}{s} & 0 \\ 0 & D_{Ls}+\frac{K_{Ls}}{s}\end{pmatrix} \tag{9}$$

The differential amplitude, which is the unique function of TDA-TVD, is represented by an only non-diagonal matrix $\boldsymbol{B}$. From the three equations, the block diagrams could be obtained as shown in Fig. 3.

2.2. Derivation of Linear Model of TDA-TVD on Normal Mode

The previous study [8] delivered a linearized normal model by assuming $T_{RL} = T_{LL} = 0$ and $J_{RL} = J_{LL} = J_w + r^2M/2$, i.e., which is in the case the vehicle is proceeding on straight paths and the wheels are not slipping. From the linearized model (i.e. linear load model as shown above), transfer functions of TDA-TVD could be also represented by matrices effectively. From the equations (1), (2), and (3), we have the following equation

$$\boldsymbol{T_{ds}} = \left[\boldsymbol{B}^T\boldsymbol{G}\boldsymbol{P_M^{-1}}\boldsymbol{G}\boldsymbol{B}(\boldsymbol{P_{ds}^{-1}}+\boldsymbol{P_L})+\boldsymbol{E_2}\right]^{-1}\boldsymbol{T_{in}} \tag{10}$$
$$= \begin{pmatrix}\frac{T_{Rds}}{T_{Rin}} & \frac{T_{Rds}}{T_{Lin}} \\ \frac{T_{Lds}}{T_{Rin}} & \frac{T_{Lds}}{T_{Lin}}\end{pmatrix}\boldsymbol{T_{in}} = \begin{pmatrix}g_{11} & g_{12} \\ g_{21} & g_{22}\end{pmatrix}\boldsymbol{T_{in}} \tag{11}$$

where $\boldsymbol{E_2}$ is an 2x2 identity matrix. Each component of the matrix above is the transfer function between $T_{R(L)in}$ and $T_{R(L)ds}$. These matrices representation can handle different left and right side parameters, but for the practicality, they are designed to be as equal as possible.

Now we assume all the left and right side parameters except for

b_1 and b_2 are equal (e.g., $G_R = G_L = G$, $K_{Rs} = K_{Ls} = K_s$, etc.). In that case, $\boldsymbol{G}$, $\boldsymbol{P_{ds}}$, $\boldsymbol{P_M}$, and $\boldsymbol{P_L}$ become scalars. The above equation will become

$$\boldsymbol{T_{ds}} = [X\boldsymbol{Z} + \boldsymbol{E_2}]^{-1}\boldsymbol{T_{in}} \tag{12}$$

where

$$\boldsymbol{Z} = \begin{pmatrix} Z_{11} & Z_{12} \\ Z_{21} & Z_{22} \end{pmatrix} = \boldsymbol{B}^T\boldsymbol{B} \tag{13}$$

$$= \begin{pmatrix} (b_2+1)^2 + b_1^2 & -b_1^2 - b_1 - b_2^2 - b_2 \\ -b_1^2 - b_1 - b_2^2 - b_2 & (b_1+1)^2 + b_2^2 \end{pmatrix}, \tag{14}$$

and

$$X = G^2 P_M^{-1}(P_{ds}^{-1} + P_L) \tag{15}$$

$$= \frac{G^2(J_M s + D_M)[J_L s^2 + (D_L + D_s)s + K_s]}{(J_L s + D_L)(D_s s + K_s)} = \frac{X_n}{X_d}$$

Now we get the following equation

$$\boldsymbol{T_{ds}} = \frac{X_d}{Y}\begin{pmatrix} Z_{22}X_n + X_d & -X_n Z_{12} \\ -X_n Z_{21} & Z_{11}X_n + X_d \end{pmatrix}\boldsymbol{T_{in}} \tag{16}$$

$$= \begin{pmatrix} g_{11} & g_{12} \\ g_{21} & g_{22} \end{pmatrix}\boldsymbol{T_{in}},$$

where

$$Y = X_n^2|\boldsymbol{Z}| + X_n X_d(Z_{11} + Z_{22}) + X_d^2 \tag{17}$$

$$|\boldsymbol{Z}| = (b_1 + b_2 + 1)^2 \tag{18}$$

$$Z_{11} + Z_{22} = b_1^2 + b_1 + b_2^2 + b_2 + 1. \tag{19}$$

In addition, for the later use, the following parameters are defined.

$$\boldsymbol{J} = \begin{pmatrix} J_{11} & J_{12} \\ J_{21} & J_{22} \end{pmatrix} = G^2 J_M \boldsymbol{Z} \tag{20}$$

Since left and right sides of TDA-TVD are 1DOF systems, ω_{Rds}, ω_{RL}, T_{Rds} have one-to-one-one relationships each other, which is given by the following equations (the same goes for between ω_{Lds}, ω_{LL}, T_{Lds}),

$$\boldsymbol{\omega_{ds}} = \frac{J_L s^2 + (D_L + D_s)s + K_s}{(J_L s + D_L)(D_s s + K_s)}\boldsymbol{T_{ds}} \tag{21}$$

$$\boldsymbol{\omega_L} = \frac{1}{J_L s + D_L}\boldsymbol{T_{ds}} \tag{22}$$

we can also obtain the transfer functions with the driveshaft-side angular frequency or wheel speed frequency being outputs (i.e., $\frac{\boldsymbol{\omega_{ds}}}{\boldsymbol{T_{in}}}$, $\frac{\boldsymbol{\omega_L}}{\boldsymbol{T_{in}}}$). By also using (5) and (6), we can derive other transfer functions such as $\frac{\boldsymbol{\omega_M}}{\boldsymbol{T_M}}$.

3. Dynamic Model of TDA-TVD with Summation-Differential Mode Transformation

The previous approach requires the decoupling compensator. Not only it makes the overall controller architecture more complex, but also the linearized model does not effectively consider the yaw motion, which varies the apparent load inertia. Since the behavior of the vehicle is drastically different in the both cases, it is better to construct the dynamic model of the each state respectively and their corresponding controllers. We define a summation mode in which the vehicle is translating, and a differential mode in which the vehicle is rotating in the yaw axis. The idea of coordinate transformation can be seen on [9], where mathematical operation makes it easier to handle seemingly complex plants.

3.1. Derivation of Dynamic Model of TDA-TVD with SDMT

(2) can be simplified by assuming the left and right side parameters are equal to each other (except for $b_1 \neq b_2$) as follows

$$\boldsymbol{\omega_{ds}} = G^{-2}P_M\boldsymbol{Z}^{-1}(\boldsymbol{T_{in}} - \boldsymbol{T_{ds}}) \tag{23}$$

From the above equation, it is clear that the both input torques T_{Rin} and T_{Lin} affect to the output angular speed ω_{Lds} and ω_{Rds}, since the matrix $\boldsymbol{Z}^{-1}$ is not diagonal, which is also visible in the coupling blocks in the block diagrams of TDA-TVD. If we could make this matrix diagonal by certain proper coordinate transformation, we can decouple the two of 1DOF systems.

Fundamentally, TDA-TVD is a device that further amplifies differential torque inputs. Therefore, it is natural to decouple the systems in two modes; summation and differential modes, where equal and differential input torques are applied to the left and right side wheels. In order to convert a dynamic model of TDA-TVD by summation-differential mode transformation (SMDT), we need to multiply a coordinate transformation matrix $\boldsymbol{A}$ to each of input and output parameters, which is given by

$$\boldsymbol{A} = \frac{1}{2}\begin{pmatrix} 1 & 1 \\ 1 & -1 \end{pmatrix}. \tag{24}$$

Load side dynamics are easy to perform the SMDT because there is no couplings between left and right systems.

Now, we would like to multiply (23) by $\boldsymbol{A}$ and it is given by

$$\boldsymbol{A\omega_{ds}} = \boldsymbol{A}G^{-2}P_M\boldsymbol{Z}^{-1}(\boldsymbol{T_{in}} - \boldsymbol{T_{ds}}) \tag{25}$$

$$= G^{-2}P_M\boldsymbol{C}\boldsymbol{A}(\boldsymbol{T_{in}} - \boldsymbol{T_{ds}}) \tag{26}$$

$$\begin{pmatrix} \omega_{Sds} \\ \omega_{Dds} \end{pmatrix} = G^{-2}P_M\boldsymbol{C}\begin{pmatrix} T_{Sin} - T_{Sds} \\ T_{Din} - T_{Dds} \end{pmatrix} \tag{27}$$

where $\boldsymbol{C}$ is a certain diagonal matrix to obtain. If we assume $b_1 = b_2 \approx b = (b_1 + b_2)/2$,

$$|\boldsymbol{Z}| = 4b^2 + 4b + 1 = (2b+1)^2 \tag{28}$$

$$= (b_1 + b_2 + 1)^2$$

$$Z_{11} - Z_{12} = Z_{22} - Z_{21} \tag{29}$$

$$= (2b^2 + 2b + 1) - (-2b^2 - 2b)$$

$$= 4b^2 + 4b + 1 = |\boldsymbol{Z}|$$

$$Z_{11} + Z_{12} = Z_{22} + Z_{21} \tag{30}$$

$$= (2b^2 + 2b + 1) + (-2b^2 - 2b) = 1$$

therefore,

$$\boldsymbol{C} = \begin{pmatrix} 1 & 0 \\ 0 & \frac{1}{|\boldsymbol{Z}|} \end{pmatrix} = \begin{pmatrix} 1 & 0 \\ 0 & \frac{1}{(b_1+b_2+1)^2} \end{pmatrix}. \tag{31}$$

The above equation is a diagonal matrix, which means that the each mode is decoupled from each other.

Now we have the block diagram of TDA-TVD in both the summation and differential modes as shown in Fig. 4(a) and Fig. 4(b). The unique feature of the torque differential amplification only appears on the differential mode and not on the summation mode, which agrees with the intended function of TDA-TVD.

3.2. Derivation of Linear Model of TDA-TVD on Summation Mode

A linearization of the dynamic model of TDA-TVD on summation and differential modes is required to construct controllers.

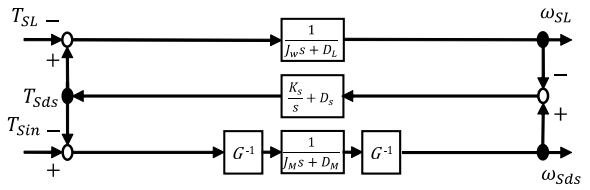

(a) Summation mode.

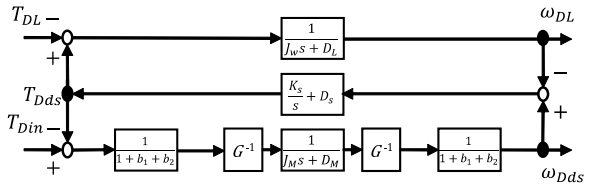

(b) Differential mode.

Fig. 4 Block diagrams of linearized normal model of TDA-TVD.

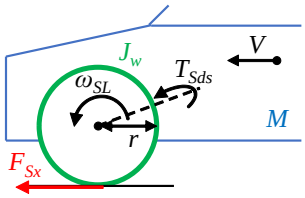

Fig. 5 Accelerating vehicle.

The linearization here means the load torque T_L is solely determined by the input torque T_{in} so that T_L can be replaced by an equivalent load side dynamics. On the summation mode, we consider the vehicle accelerating on straight paths as shown in Fig. 5.

We have the following equations to describe the acceleration of the wheels and vehicle

$$\omega_{SL} = \frac{1}{J_w s + D_L}(T_{Sds} - T_{SL}) \tag{32}$$
$$T_{SL} = rF_{Sx} \tag{33}$$
$$V_x = \frac{2}{Ms}F_{Sx} \tag{34}$$
$$V_{SL} = r\omega_{SL} \tag{35}$$
$$\lambda_S = \frac{V_{SL} - V_x}{V_{SL}}, \tag{36}$$

where V_x is the longitudinal vehicle body speed and λ_S is the summation slip ratio. From these equations, we get the transfer function of the linear model as follows

$$\frac{\omega_{SL}}{T_{Sds}} = \frac{1}{(J_w + r^2M(1-\lambda_S)/2)s + D_L} = \frac{T_{Sds}}{J_{SL}s + D_L}, \tag{37}$$

where J_{SL} is the equivalent load inertia on the summation mode. The block diagram of the linearized model of TDA-TVD on the summation mode is shown in Fig. 6. In the figure, the motor inertia and viscosity on the summation mode J_{SM} and D_{SM} are given by

$$J_{SM} = G^2 J_M \tag{38}$$
$$D_{SM} = G^2 D_M. \tag{39}$$

Some of transfer functions of this summation mode are given by

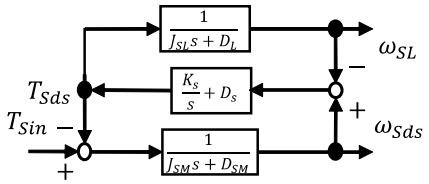

Fig. 6 Block diagram of linearized TDA-TVD in summation mode.

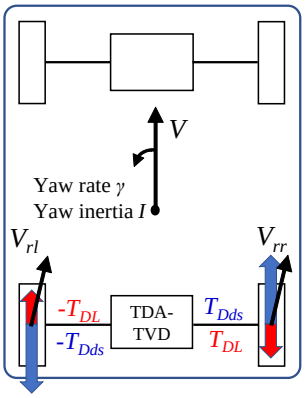

Fig. 7 Rotating vehicle.

$$\frac{T_{Sds}}{T_{Sin}} = \frac{(J_{SL}s + D_L)(D_s s + K_s)}{c_3 s^3 + c_2 s^2 + c_1 s + c_0} \tag{40}$$
$$\frac{\omega_{Sds}}{T_{Sin}} = \frac{J_{SL}s^2 + (D_L + D_s)s + K_s}{c_3 s^3 + c_2 s^2 + c_1 s + c_0} \tag{41}$$
$$\frac{\omega_{SL}}{T_{Sin}} = \frac{D_s s + K_s}{c_3 s^3 + c_2 s^2 + c_1 s + c_0} \tag{42}$$
$$c_3 = J_{SM}J_{SL} \tag{43}$$
$$c_2 = J_{SM}(D_L + D_s) + J_{SL}(D_{SM} + D_s)$$
$$c_1 = D_{SM}D_L + D_{SM}D_s + D_L D_s + K_s(J_{SM} + J_{SL}) \tag{44}$$
$$c_0 = (D_{SM} + D_L)K_s$$

3.3. Derivation of Linear Model of TDA-TVD on Differential Mode

On the differential mode, we consider the rotating vehicle as shown in Fig. 7. The left and right wheel have the different longitudinal vehicle speed from the longitudinal vehicle body speed V_x due to the yaw rate γ, which is given by

$$V_{rrx} = V_x + \frac{d}{2}\gamma \tag{45}$$
$$V_{rlx} = V_x - \frac{d}{2}\gamma. \tag{46}$$

Therefore, a differential longitudinal vehicle speed between the left and right wheels V_{Dx} is given by

$$V_{Dx} = \frac{V_{rrx} - V_{rlx}}{2} = \frac{d}{2}\gamma. \tag{47}$$

With the equation above, we can define the differential slip ratio λ_D as follows

$$\lambda_D = \frac{r\omega_{DL} - V_{Dx}}{r\omega_{DL}}. \tag{48}$$

Now, the yaw rate and the differential angular speed ω_{DL} can be

related, which is given by

$$\gamma = \frac{r}{d/2}\left(1-\lambda_D\right)\omega_{DL}. \tag{49}$$

We have the following equations to describe the yaw rotation of the wheels and vehicle

$$\omega_{DL} = \frac{1}{J_w s + D_L}\left(T_{Dds} - T_{DL}\right) \tag{50}$$

$$T_{DL} = rF_{Dx} \tag{51}$$

$$\begin{aligned} I\dot{\gamma} = &-2C_f l_f\left(\beta + \frac{l_f}{V}\gamma - \delta_f\right) \\ &+ 2C_r l_r\left(\beta - \frac{l_r}{V}\gamma\right) + \frac{d}{2}2F_{Dx} \end{aligned} \tag{52}$$

$$a_y = V(\beta s + \gamma) \tag{53}$$

Since we only considers yaw motion while on the straight paths, $\delta_f = 0$ and $a_y = 0$ hold. With these, we can derive the following transfer function

$$\frac{\omega_{DL}}{T_{Dds}} = \frac{s}{J_{DL}s^2 + D_{DL}s + K_{DL}} \tag{54}$$

$$J_{DL} = J_w + \frac{2r^2}{d^2}\left(1-\lambda_D\right)I \tag{55}$$

$$D_{DL} = D_L + \frac{4r^2}{d^2 V}\left(1-\lambda_D\right)\left(C_f l_f^2 + C_r l_r^2\right) \tag{56}$$

$$K_{DL} = \frac{4r^2}{d^2}\left(1-\lambda_D\right)\left(C_r l_r - C_f l_f\right). \tag{57}$$

where J_{DL}, D_{DL}, and K_{DL} are the equivalent load inertia, load damping factor, and load elasticity factor on the differential mode. If the vehicle is neutral steer (NS), then $K_{DL} = 0$ satisfies. The block diagram of the linearized model of TDA-TVD on the differential mode is shown in Fig. 8. In the figure, the motor inertia and viscosity on the differential mode J_{DM} and D_{DM} are given by

$$J_{DM} = G^2(1+b_1+b_2)^2 J_M \tag{58}$$

$$D_{DM} = G^2(1+b_1+b_2)^2 D_M. \tag{59}$$

Some of transfer functions of this differential mode of the NS vehicle ($K_{DL} = 0$) are given by

$$\frac{T_{Dds}}{T_{Din}} = \frac{(J_{DL}s + D_{DL})(D_s s + K_s)}{d_3 s^3 + d_2 s^2 + d_1 s + d_0} \tag{60}$$

$$\frac{\omega_{Dds}}{T_{Din}} = \frac{J_{DL}s^2 + (D_{DL}+D_s)s + K_s}{d_3 s^3 + d_2 s^2 + d_1 s + d_0} \tag{61}$$

$$\frac{\omega_{DL}}{T_{Din}} = \frac{D_s s + K_s}{d_3 s^3 + d_2 s^2 + d_1 s + d_0} \tag{62}$$

$$d_3 = J_{DM}J_{DL} \tag{63}$$

$$d_2 = J_{DM}(D_{DL}+D_s) + J_{DL}(D_{DM}+D_s) \tag{64}$$

$$d_1 = D_{DM}D_{DL} + D_{DM}D_s + D_{DL}D_s \tag{65}$$

$$+ K_s(J_{DM}+J_{DL}) \tag{66}$$

$$d_0 = (D_{DM}+D_{DL})K_s \tag{67}$$

Naturally, the summation can be represented by the same way.

3.3.1. Infinite Load Inertia Approximation for Differential Mode

It is convenient to consider a differential mode with an assumption that load inertia is infinite and differential wheel speed $\omega_{DL} = 0$ because we can approximately represent the differential mode using much less parameters with descent agreement in case of low speed. Therefore, we can have the following block diagram (Fig. 9).

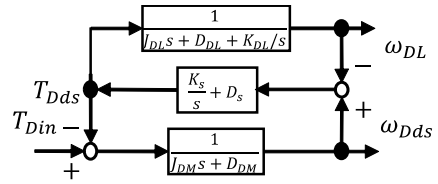

Fig. 8 Block diagram of linearized TDA-TVD in differential mode.

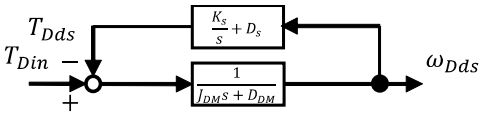

Fig. 9 Block diagram of linearized TDA-TVD in differential mode with infinite load side inertia approximation.

The transfer functions of this model are given by

$$\frac{T_{Dds}}{T_{Din}} = \frac{D_s s + K_s}{J_{DL}s^2 + (D_{DM}+D_s)s + K_s} \tag{68}$$

$$\frac{\omega_{Dds}}{T_{Din}} = \frac{s}{J_{DL}s^2 + (D_{DM}+D_s)s + K_s}. \tag{69}$$

3.4. Frequency Response Analysis of TDA-TVD on Differential Mode

In order to evaluate the proposed linear model of TDA-TVD on differential mode, simulations of frequency response of TDA-TVD with a realistic vehicle model was carried out. The realistic vehicle model contains a brush model which has a nonlinear relation between the slip of the wheel and the tire force. The simulated vehicle has the same parameters with the experimental vehicle. Input differential torque has the amplitude of 100 Nm. Initial vehicle speed V is set to 10 m/s. The tire has an optimal slip ratio λ_{pt} of 0.1. The vehicle is assumed to be NS (or $K_{DL} = 0$). The realistic nonlinear model, the obtained linear vehicle model on the differential mode and the simplified model with infinite load side inertia are compared together. The simulated frequency response $\frac{\omega_{Dds}}{T_{Din}}$ is shown in Fig. 10.

The proposed linear models have decent agreement with the nonlinear vehicle model above 1Hz on the gain diagram. In that case, the infinite load side inertia approximation model is enough to consider the higher frequency response. However, the infinite load side inertia approximation model has a considerable difference at the lower frequency region. Overall, the proposed linear model on the differential mode of TDA-TVD is reasonable to emulate the real hardware.

The simulated frequency response $\frac{T_{Dds}}{T_{Din}}$ is shown in Fig. 11. In this figure, the realistic nonlinear model, the obtained linear model on the differential mode and the same linear model with the assumption $K_{DL} = 0$, $D_{DL} = D_L$. The latter linear model is convenient to design a joint torque vibration suppression controller since no parameters related to the tire are needed and therefore also compared here.

Except for the difference of the peak amplitude at the resonance frequency around 2Hz, the both linear models have decent agreement with the realistic nonlinear model. Thus, the linear model with the assumption $K_{DL} = 0$, $D_{DL} = D_L$ is used for the controller design.

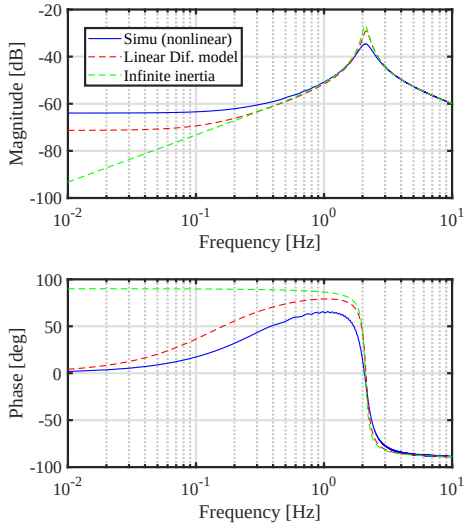

Fig. 10 Bode diagram of TVD with infinite load inertia on differential mode $\frac{\omega_{Dds}}{T_{Din}}$ ($V = 10$ m/s, λ_{pt}=0.1).

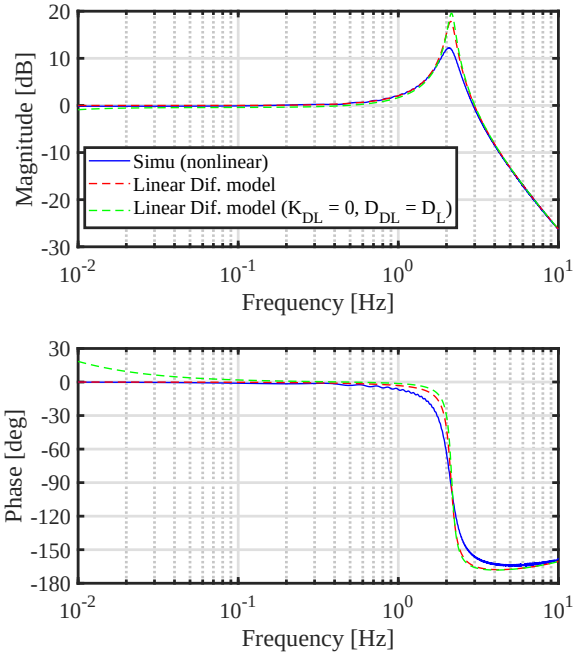

Fig. 11 Bode diagram of TVD with infinite load inertia on differential mode ($V = 10$ m/s, λ_{pt} = 0.1).

Table 1 Nominal parameters of experimental vehicle with TDA-TVD unit.

M	2173 kg
J_M, J_w, I	0.0183, 1.81, 3308 kg·m^2
K_s	6723.1 N/rad
r, d	0.338, 1.54 m
G, b_1, b_2	10.8, 0.892, 0.895

Table 2 Identified fitting parameters.

D_M, D_s, D_L	0.1, 15, 1.25 N/(rad/s)
K_s	6723.1×0.43 N/rad

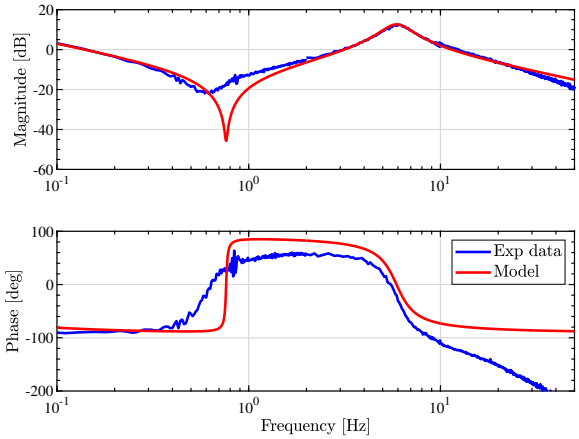

(a) Frequency response of $\frac{\omega_{SM}}{T_{SM}}$ There are a resonance at 6 Hz and an anti-resonance at 0.6 Hz in this model.

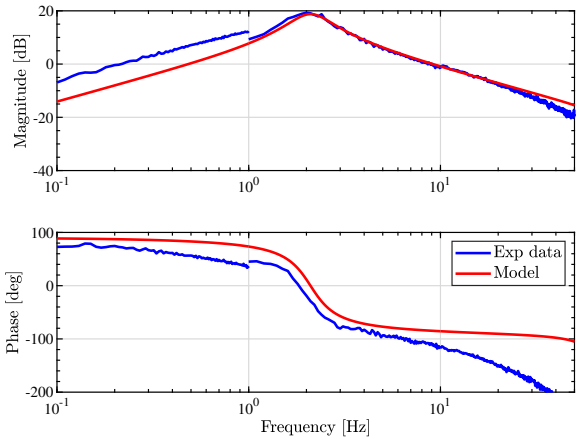

(b) Frequency response of $\frac{\omega_{DM}}{T_{DM}}$ There is a resonance at 2 Hz in this model.

Fig. 12 Frequency response of TDA-TVD on summation and differential modes.

3.5. Frequency-domain System Identification of TDA-TVD on Summation-Differential Mode

An experiment of the frequency response identification of a real TDA-TVD unit was carried out. The TDA-TVD unit is connected with two individual load motor to emulate a vehicle translating and not turning, without the slip of wheels. The following parameters shown in Tab. 2 were used to get the frequency response of the obtained summation and differential models.

The experimental results of the frequency response identification are shown in Fig. 12(a) and Fig. 12(b). The identified frequency responses are $\frac{\omega_{SM}}{T_{SM}}$ and $\frac{\omega_{DM}}{T_{DM}}$. In the both cases, the gain and phase diagrams show certain agreement between the experimental results and obtained linear models.

The reason why the phase decreases at higher frequency in case of the experiments is because of sampling frequency of 100 Hz. The experiment of the system identification on differential mode was carried out on two frequency intervals from 0.01 to 1.0 Hz and 1.0 to 100 Hz separately. That is why the curves of the experimental data are not continuous at 1 Hz.

SDMT enables us to construct vehicle dynamics controller much easier since we do not need to take the coupling between

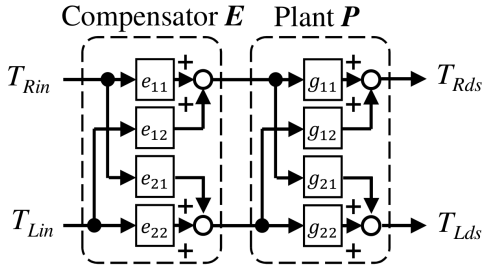

Fig. 13 Decoupling compensator E is inserted before TDA-TVD (Plant P).

the left and right wheels into account.

Now, two of vibration suppression controllers are proposed in this chapter.

4. Design of Joint Torque Controller

4.1. Conventional Feedforward Controller using Decoupling Compensator

The previous study designed a decoupling compensator $\boldsymbol{E}$ based on an "diagonalization" as shown in Fig. 13 and the following equations

$$e_{11} = e_{22} = 1 \tag{70}$$
$$e_{12} = -\frac{g_{12}}{g_{11}} \tag{71}$$
$$e_{21} = -\frac{g_{21}}{g_{22}}. \tag{72}$$

The previous study assumed a load inertia to be that of the summation mode, i.e., $J_{RL} = J_{LL} = J_{SL}$, and $D_M = D_L = 0$. The transfer functions with the decoupling compensator $\boldsymbol{E}$ are obtained as follows

$$\frac{T_{Rds}}{T_{Rin}} = \frac{J_{LS}(D_s s + K_s)}{J_{11}J_{LS}s^2 + D_s J_{X1} s + K_s J_{X1}} \tag{73}$$
$$\frac{T_{Rds}}{T_{Lin}} = \frac{T_{Lds}}{T_{Rin}} = 0 \tag{74}$$
$$\frac{T_{Lds}}{T_{Lin}} = \frac{J_{LS}(D_s s + K_s)}{J_{22}J_{LS}s^2 + D_s J_{X2} s + K_s J_{X2}} \tag{75}$$
$$J_{X1} = J_{11} + J_{LS}, J_{X2} = J_{22} + J_{LS}$$

The joint torque control feedforward controller with the decoupling compensator (JTC-FF-E) was constructed by the inverse of the above equations multiplied by an additional filter in the same way (see Fig. 14(b))

4.2. Proposed Feedforward Controller using SDMT

This section designs a joint torque vibration suppression control based on SDMT. We utilize (40) and (60) to construct the feedforward of the joint torque controller based on SDMT (JTC-FF-S(D)) given by

$$C_{JTC-FF-S} = \frac{T_{Sin}}{T_{Sds}} \frac{1}{\tau s + 1} \tag{76}$$
$$= \frac{c_3 s^3 + c_2 s^2 + c_1 s + c_0}{(J_{SL}s + D_{SL})(D_s s + K_s)(\tau s + 1)}$$
$$C_{JTC-FF-D} = \frac{T_{Din}}{T_{Dds}} \frac{1}{\tau s + 1} \tag{77}$$
$$= \frac{d_3 s^3 + d_2 s^2 + d_1 s + d_0}{(J_{DL}s + D_L)(D_s s + K_s)(\tau s + 1)},$$

where τ is a cutoff frequency of an additional filter to make the transfer functions proper. The overall block diagram of the joint torque controller including the coordinate transformation is shown in Fig. 14(a).

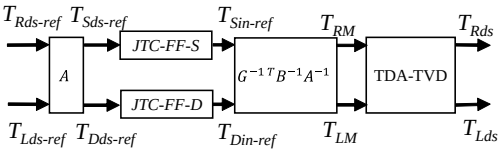

(a) Based on Summation-Differential mode transformation (Prop.).

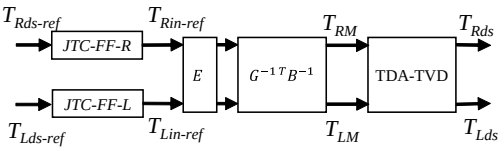

(b) Based on decoupling compensator $\boldsymbol{E}$ (Conv.).

Fig. 14 Implemented block diagrams of Joint torque controllers.

5. Experiemtnal Verification of Joint Torque Vibration Suppression Control

In this section, an experimental verification of the joint torque vibration suppression control is carried out. To evaluate the effectiveness of the proposed controller, three cases are compared; without any control (wo control), JTC based on SDMT (JTC-FF-S or JTC-FF-D), and JTC based on the normal mode with the decoupling compensator (JTC-FF-E).

5.1. Experimental Conditions

The following two scenarios are verified on a straight dry path, and the steering angle is held at 0 degree by a driver in the whole experiment. The first scenario is that the vehicle is driven by the differential driveshaft torque reference of $450\,\mathrm{Nm}$ when the vehicle is running at $45\,\mathrm{km/h}$. The second scenario is that the vehicle is accelerated by the summation driveshaft torque reference of $500\,\mathrm{Nm}$ when the vehicle is running at $20\,\mathrm{km/h}$.

The experimental vehicle with TDA-TVD is shown in Fig. 15. TDA-TVD drives rear wheels using two electric motors. The driving control unit uses MicroAutoBox (MAB) to output drive shaft torque command which is determined by accelerator opening degree and vehicle speed. MAB communicates with Motor Control Unit (MCU) by Controller Area Network (CAN) in a cycle of $10\,\mathrm{ms}$. The controllers of JTC are implemented on the MCU. The drive shaft torque command is input to the JTC controllers through a low-pass filter, whose cutoff frequency is $10\,\mathrm{Hz}$. The torque command is calculated in a cycle of $1\,\mathrm{ms}$. To protect TDA-TVD, the drive shaft torque command differential rate is limited by $1000\,\mathrm{Nm/s}$.

5.2. Experimental Results

Fig. 16 shows the experimental results with different JTC controllers. As shown in Fig. 16(a) the experimental results on differential mode, the drive shaft torque vibrates at $2\,\mathrm{Hz}$ when the differential torque is applied without control. It is caused by the torsional resonance of the drive shaft on the differential mode as shown in section IV. On the other hand, the vibration can be suppressed by the controller of JTC-FF-E with tuned parameters. Even though JTC-FF-D with nominal and identified parameters in Tab. 1 and Tab. 2 has a constant error about $100\,\mathrm{Nm}$, it

Fig. 15 Experimental vehicle equipped with TDA-TVD. TDA-TVD drives rear wheels using two electric motors.

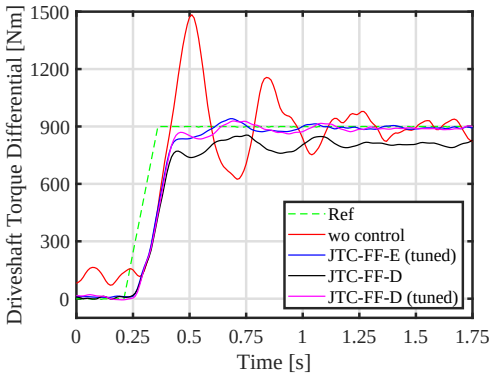

(a) Differential mode.

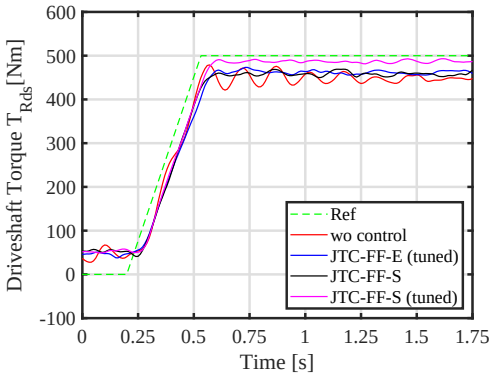

(b) Summation mode.

Fig. 16 Experimental results of Joint Torque Suppression.

could be reduced by tuning the parameters during the experiment. The controller of JTC-FF-D with tuned parameters obtained almost the same vibration suppression performance with JTC-FF-E (tuned).

Fig. 16(b) shows the experimental results with different JTC controllers on summation mode. The drive shaft torque vibrates at 6 Hz when the summation torque is applied. It is caused by the torsional resonance of drive shaft on summation mode. The vibration can be suppressed by the controllers of JTC-FF-E (tuned) and JTC-FF-S, but there is a constant error about 30 Nm. This error decreases to about 10 Nm after tuning the parameters of the controller. Comparing with JTC-FF-E (tuned), there is lower model error in JTC-FF-S (tuned), because JTC-FF-E (tuned) does not consider the viscosity coupling.

6. Conclusion

This study proposed a novel linearized model of TDA-TVD that well describes the longitudinal motion (summation mode) and yaw motion (differential mode) using a coordinate transformation and analyzes TDA-TVD in the frequency domain in detail. By splitting into summation and differential modes, the frequency domain analysis of the real hardware of TDA-TVD becomes much easier. Furthermore, the driveshaft torque vibration of the summation and differential modes could be effectively mitigated by designing controllers for the corresponding modes. In this paper, a driveshaft torque vibration suppression controller is designed based on the inverse model of summation and differential modes. To evaluate the effectiveness of the proposed controller, simulation and experiment verification are carried out. The evaluation results show that summation and differential modes define the TDA-TVD model more precisely, so that the proposed method has less model error. An improved and more detailed system identification of TDA-TVD such as implementation of an additional feedback controller, and further improvement of the vibration reduction will be future work.

References

(1) Y. Shibahata, K. Shimada, and T. Tomari, “Improvement of vehicle maneuverability by direct yaw moment control”, Veh. Syst. Dyn., vol. 22, no. 5-6, pp. 465-481, 1993.

(2) K. Sawase, Y. Ushiroda, and T. Miura, “Left-right torque vectoring technology as the core of super all wheel control (S-AWC)”, Mitsubishi Motors Tech. Rev., vol. 18, pp. 16-23, 2006.

(3) Y. Hori, “Future vehicle driven by electricity and control research on four-wheel-motored ‘UOT electric march II’”, IEEE Trans. on Industrial Electronics, 51, 5, pp. 954-962, 2004.

(4) Sawase. K, Chiba M, “Study of Lateral Torque-vectoring Differential Suitable for Electric Powered Vehicles”, Transactions of Society of Automotive Engineers of Japan, Vol.45-5, p.823-828, 2014 (In Japanese).

(5) Sawase. K, et.al., “Classification and Analysis of Torque-vectoring Differentials with Torque Difference Amplification Mechanism”, Transactions of Society of Automotive Engineers of Japan, Vol.48, No.2, p.317-322, 2017 (In Japanese).

(6) J. Zhang, W. Sun and H. Du, “Integrated Motion Control Scheme for Four-Wheel-Independent Vehicles Considering Critical Conditions”, in IEEE Transactions on Vehicular Technology, vol. 68, no. 8, pp. 7488-7497, Aug. 2019.

(7) M. Chae, Y. Hyun, K. Yi and K. Nam, “Dynamic Handling Characteristics Control of an in-Wheel-Motor Driven Electric Vehicle Based on Multiple Sliding Mode Control Approach”, in IEEE Access, vol. 7, pp. 132448-132458, 2019.

(8) H. Fuse, H. Fujimoto, K. Sawase, N. Takahashi, R. Takahashi, Y. Okamura, R. Koga, “Derivation of Dynamic Model of Two-Input-Two-Output Torque Difference Amplification Motor Drive System and Independent Left-and-Right Wheel Control with Decoupling Compensator”, IEEJ Journal of Industry Applications, Vol. 11, No. 3, pp. 427-436, 2022.

(9) S. Katsura and K. Ohnishi, “Quarry of Modal Information from Environment for Advanced Motion Control”, IEEJ Transactions on Industry Applications, vol. 126, no. 4, pp. 372-378, 2006.